Contents lists available at ScienceDirect

Composites Science and Technology

journal homepage: www.elsevier.com

Synergetic enhancement of mechanical and electrical strength in epoxy/silica nanocomposites via chemically-bonded interface

He Li[a, b], Feihua Liu[b], Huidong Tian[a], Chuang Wang[a], Zihao Guo[a], Peng Liu[a], Zongren Peng[a, **], Qing Wang[b, *]

[a] State Key Laboratory of Electrical Insulation and Power Equipment, School of Electrical Engineering, Xi'an Jiaotong University, Xi'an, 710049, China
[b] Department of Materials Science and Engineering, The Pennsylvania State University, University Park, 16802, USA

ARTICLE INFO

Keywords:
Polymer nanocomposites
Organic–inorganic interface
Electrical properties
Mechanical properties
Interaction zone model

ABSTRACT

While the incorporation of the inorganic fillers into polymers is envisioned to improve the properties of polymers, the organic–inorganic interface in the nanocomposite plays a prominent role in the modulation of the electrical, mechanical and thermal properties. Here, the epoxy chain-grafted silica nanoparticles were prepared and utilized as the fillers in epoxy matrix. The multiple physical properties such as the tensile strength, the elongation at break, the glass transition temperature, the dielectric strength of the nanocomposites with epoxy chain-grafted silica are simultaneously improved in comparison with those of the neat epoxy and the nanocomposites with unmodified silica. Moreover, substantial reductions in the water absorption ratio, dielectric loss and electric conductivity are obtained in the nanocomposites filled with epoxy-grafted silica even at relatively low filler loadings. These results verify the critical role of the chemically-bonded interface between organic and inorganic phases in determining the mechanical and dielectric strength of the polymer nanocomposites. The interaction zone models for the interface between nanoparticle and polymer matrix have been proposed to rationalize the experimental results.

1. Introduction

Epoxy resin is a class of thermosetting polymers that are commonly used in electronics and power systems, i.e., as packaging materials for electronic encapsulation, as structural and insulating materials for high-voltage dry-type bushing and high-voltage transformer, and as coating layers for high-voltage gas insulated switchgear [1–4]. With the miniaturization of advanced electronics and the continuous increase of power capacity and transmission voltage level, the epoxy-based insulating materials with high performance such as enhanced toughness, adhesion strength, dielectric strength and water resistance, for electronic devices and electrical equipment are urgently needed [2,4].

Recently, the composite approach, i.e. incorporation of organic and inorganic fillers into polymer matrix, has been utilized to improve the physical properties of epoxy resin [5–8]. The introduction of nanofillers including silica, alumina, aluminum nitride, boron nitride, barium titanate and carbon nanotubes into the epoxy resin not only retains the original excellent performance of pristine polymer, but also greatly expands its applications because of enhanced electrical, mechanical and thermal properties [2,7–15]. However, it needs to be pointed out that the significantly different physical and chemical properties between inorganic nanoparticles and resin matrix result in poor interfacial compatibility. For instance, the incorporation of inorganic nanoparticles is prone to introduce defects, such as pores and micro-cracks, into the nanocomposite [16,17]. In addition, agglomeration of the fillers is known to lead to much degraded properties of the resultant composites [18]. Thus, to design compatible and intimate inorganic–organic interfaces in polymer nanocomposites, numerous surface modification methods for nanoparticles including hydroxylation, silanization and esterification have been carried out [8,16,19–26]. For instance, organic chains have been bonded onto the surface of the nanoparticles via a silicon–oxygen–silicon bond with a silane coupling agent [9,11,19,20,27]. However, the compatibility between the silane coupling agent modified nanoparticles and epoxy resin is only improved over a rather limited range due to the different molecular structures between the coupling agent and the host polymer [27].

Herein we describe the utilization of the silica nanoparticles with chemically-bonded interfaces in the epoxy nanocomposite to synergis-

* Corresponding author.
** Corresponding author.
Email addresses: zrpeng@xjtu.edu.cn (Z. Peng); wang@matse.psu.edu (Q. Wang)

https://doi.org/10.1016/j.compscitech.2018.08.047
Received 2 June 2018; Received in revised form 11 August 2018; Accepted 30 August 2018
Available online xxx
0266-3538/

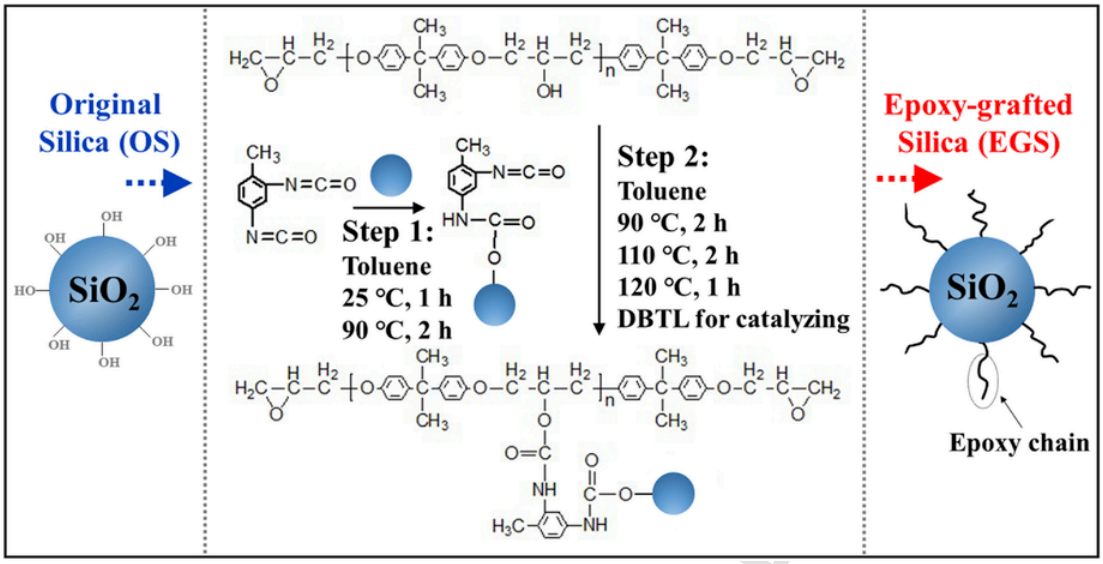

Fig. 1. Synthesis of chemically-bonded EGS particles.

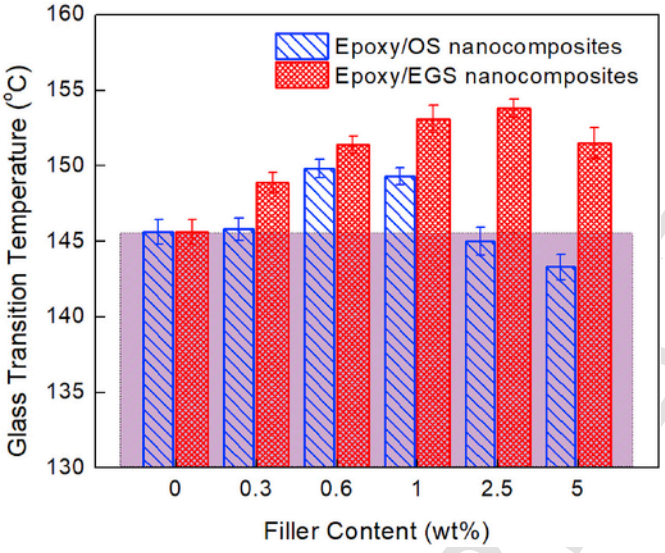

Fig. 2. Glass transition temperatures of neat epoxy and the nanocomposites.

tically enhance the multiple properties including tensile strength, electrical breakdown strength, arc ablation resistance and water absorption resistance when compared to neat polymer and the polymer nanocomposites with unmodified silica. The enhancements have been attributed to the chemically grafted-epoxy chains onto the surface of the nanoparticles, which not only improve the physical compatibility between the epoxy matrix and the nanofiller due to the same chemical structures but also provide the chemistries for establishment of the cross-linked networks during the cross-linking reaction. Additionally, an interaction zone model for the organic–inorganic interface in polymer nanocomposites has been proposed to rationalize the experimental results.

2. Experimental

2.1. Materials

Silica nanoparticles with an average diameter of 30 ± 5 nm and a specific surface area of $220 \pm 30\,m^2/g$ was purchased from Hangzhou Wanjin New Material Co., Ltd. China. 2,4-Toluene diisocyanate (TDI) was purchased from Sinopharm Chemical Reagent Co., Ltd. China. Diglycidyl ether of bis phenol A (DGEBP-A) type epoxy resins (E-39 and E-51) were purchased from Wuxi Resin Co., Ltd. China. The curing agent, methylhexahydrophthalic anhydride (MeHHPA), was purchased

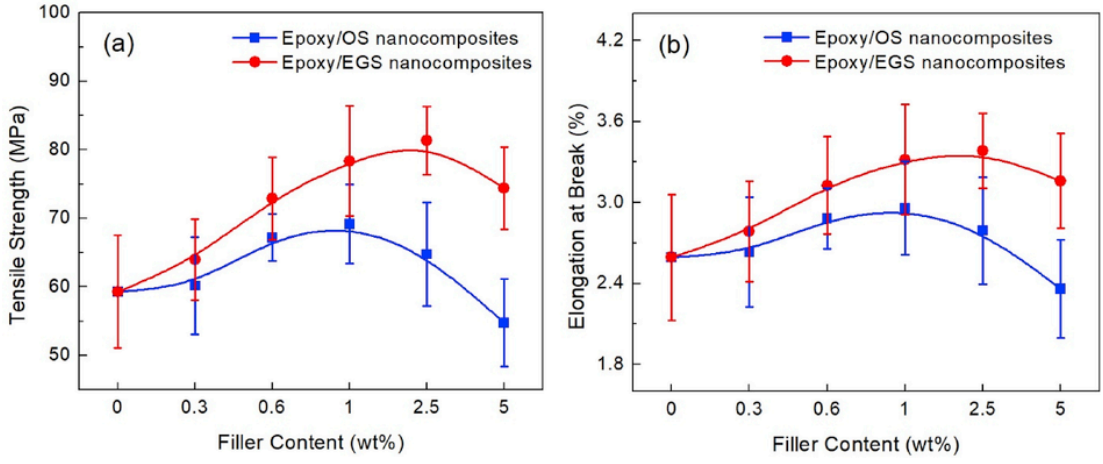

Fig. 3. (a) Tensile strength and (b) elongation at break of neat epoxy and the nanocomposites with varied silica contents.

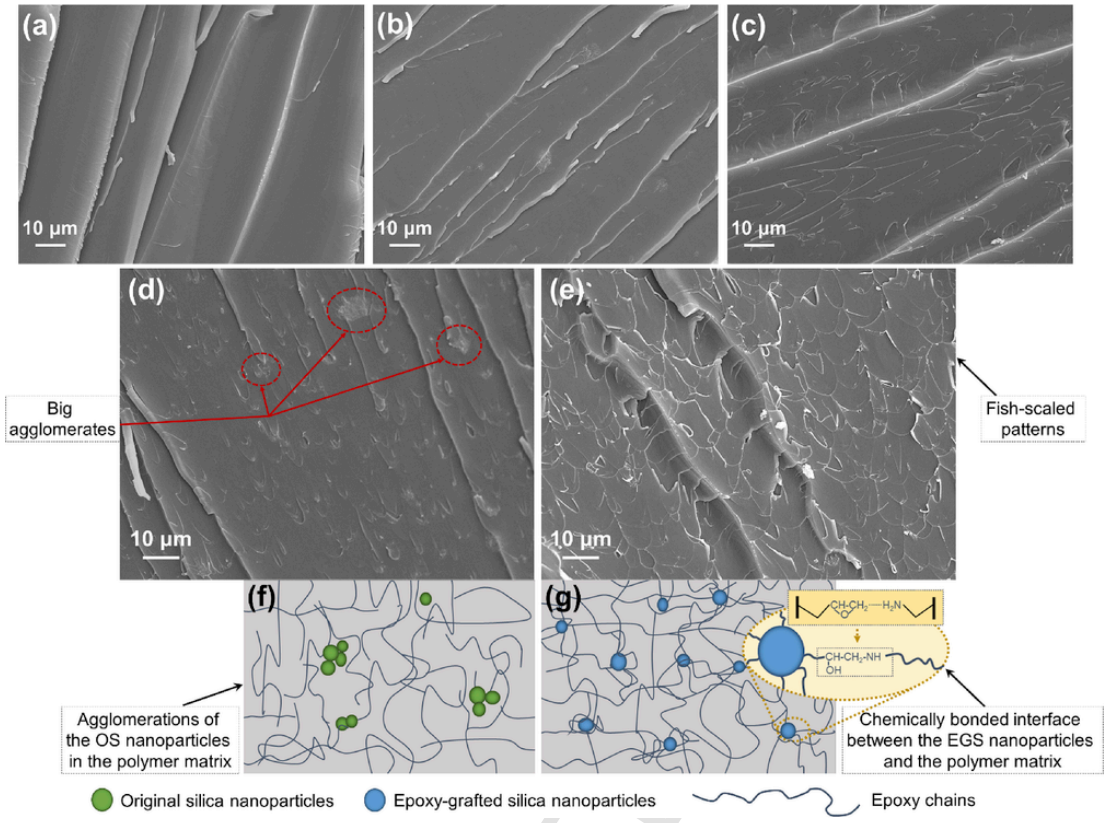

Fig. 4. Cross-sectional SEM images of (a) neat epoxy, (b) epoxy nanocomposite with 0.6 wt% OS; (c) epoxy nanocomposite with 0.6 wt% EGS, (d) epoxy nanocomposite with 2.5 wt% OS and (e) epoxy nanocomposite with 2.5 wt% EGS; Schematic illustrations of (f) epoxy/OS nanocomposite structures and (g) epoxy/EGS nanocomposite with chemically-bonded structures.

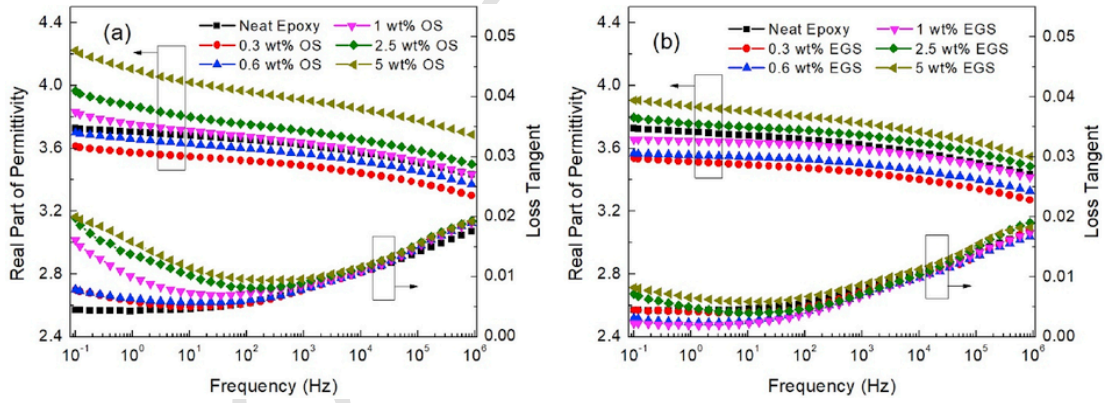

Fig. 5. Frequency dependence of the real part of permittivity and loss tangent of the (a) epoxy/OS composites and (b) epoxy/EGS composites with varied silica contents.

from Fuyang Huicheng Electronic Material Co., Ltd. China. The curing accelerator, 2-ethyl-4-methylimidazole, was purchased from Nanjing Zhengri Chemical Co., Ltd. China. Xylene, toluene, dibutyltin dilaurate (DBTL), dimethylbenzene, butyl alcohol, ethanol and acetone were in analysis purity and purchased from Chemical Reagent Co., Ltd. China.

2.2. Preparation of epoxy-grafted silica

Firstly, 10 g silica nanoparticles were dispersed in toluene with magnetic stirring followed by ultrasonication for 30 min to make a homogeneous mixture. The mixture was then heated at 135 °C for 2 h under nitrogen atmosphere. After cooling to room temperature, 5 g TDI was slowly added into the mixture with magnetic stirring for 1 h to make a homogeneous mixture. After reaction at 90 °C for 2 h, the products were repetitively washed and centrifuged three times with acetone to remove physically adsorbed TDI molecules. The TDI-grafted nano-silica (T-silica) was obtained after drying at 40 °C in a vacuum oven for 12 h. Secondly, 12 g dehydrated epoxy resin was added to a flask and heated to 120 °C for 2 h and then treated at 60 °C under a nitrogen atmosphere overnight. 80 g toluene was injected into the flask while maintaining stirring until the epoxy resin dissolved to form a homogeneous mixture. T-silica particles and 0.12 g DBTL were added to the mixture. The reaction was performed at 90 °C for 2 h, 110 °C for 2 h and 120 °C for 1 h. The products were repetitively washed and centrifuged three times with acetone and were dried at 40 °C for 12 h in a vacuum oven. The chemically-bonded nanoparticles with the epoxy molecules were marked as epoxy-grafted silica (EGS). The unmodified silica nanoparticles were designated as original silica (OS). Schematic

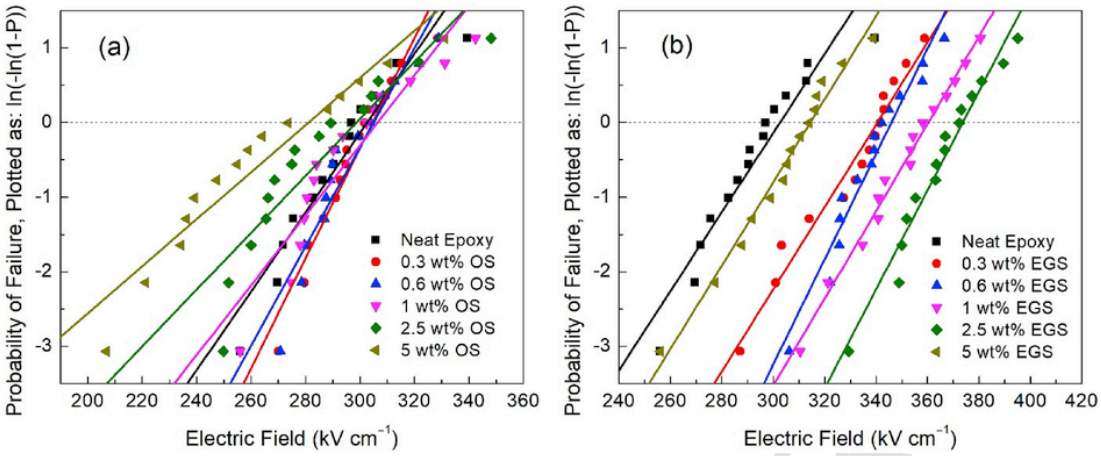

Fig. 6. Weibull electrical breakdown strength of neat epoxy and the nanocomposites with varied silica contents.

Table 1
The scale parameter (α) and the shape parameter (β) from the Weibull statistics of neat epoxy and the nanocomposites with varied silica contents.

	Epoxy/OS nanocomposites		Epoxy/EGS nanocomposites	
	α (kV cm^{-1})	β	α (kV cm^{-1})	β
Neat epoxy	302.7	15.82	/	/
0.3 wt%	304.6	22.09	341	17.71
0.6 wt%	305	19.99	346.4	23.87
1 wt%	306.5	14.19	360.7	20.22
2.5 wt%	298.7	11.36	374.1	24.12
5 wt%	281	8.49	314.9	16.48

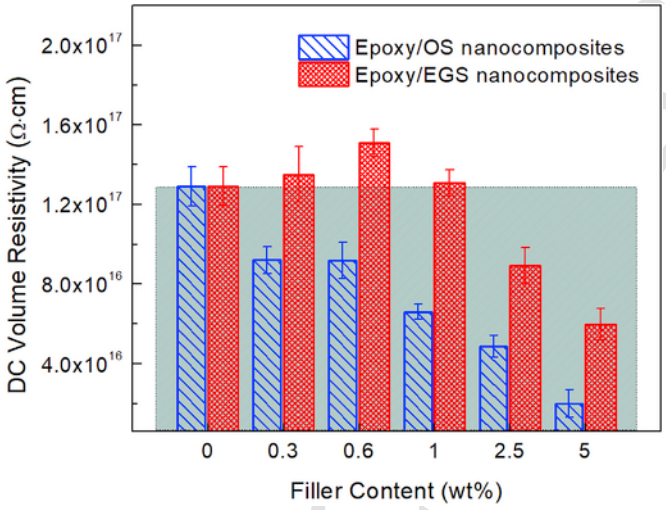

Fig. 7. DC volume resistivity of neat epoxy and the nanocomposites with varied silica contents.

illustrations of the chemical reactions for the EGS preparation are shown in Fig. 1.

2.3. Preparation of composites

The epoxy resin was dissolved separately in a mixed solution of xylene and butyl alcohol at room temperature. Subsequently, 0.3, 0.6, 1, 2.5 and 5% by weight of OS and 0.35, 0.7, 1.17, 2.93 and 5.85% by weight of EGS particles were added into the epoxy resin solution with magnetic stirring for 0.5 h. Next, the mixtures were dispersed by a mechanical agitation at a speed of 8000 r m^{-1} for 30 min and followed by ultrasonication for another 30 min and then under vacuum for pre-degassing. For comparison, a neat epoxy formulation was also fabricated. The different nanocomposite formulations as well as neat epoxy formulation were obtained with a mass ratio of 100:85:0.5 of epoxy resin to curing agent to curing accelerator for stoichiometric reactions. All formulations were homogenized with mechanical stirring for 30 min and then vacuumed again before the curing processes. The bulk specimens were fabricated by pouring the liquid formulation into re-treated molds, and the coating-glass specimens were fabricated by brushing the liquid formulation onto the surface of slide glass. After degassing at 60 °C for 1 h and 80 °C for 1 h in a vacuum oven, the specimens were cured in an air-circulating oven at 110 °C for 3 h and 150 °C for 6 h. Last, the specimens were stepwise cooled down to room temperature to relieve the internal stress of the materials. The thickness of bulk specimens for dielectric spectroscopy measurement, electrical breakdown strength test and arc ablation resistance test were around 0.5 mm, 0.8 mm and 1.5 mm, respectively. The dimension of the glass slide was 20 mm × 20 mm × 2 mm for the water absorption test. The specimens for dielectric spectroscopy were gold coated with Φ 30 mm for one side and Φ 40 mm for the other side.

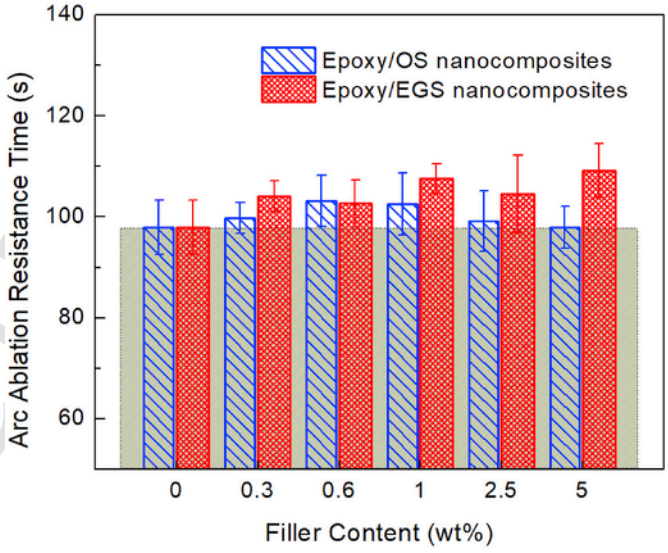

Fig. 8. Arc ablation resistance time of neat epoxy and the nanocomposites with varied silica contents.

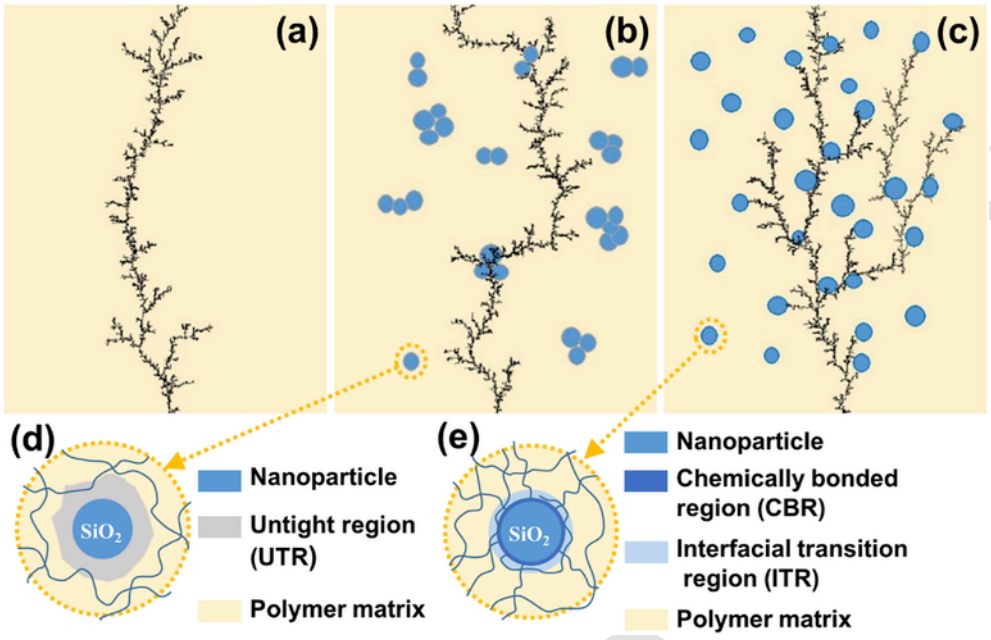

Fig. 9. The schematic diagrams of discharge channel growth in electrical breakdown processes (a) neat epoxy, (b) epoxy/OS nanocomposite and (c) epoxy/EGS nanocomposite; The interaction zone models for (d) OS particle–epoxy matrix and (e) EGS particle–epoxy matrix.

2.4. Characterization

Fourier transform infrared (FT-IR) spectrum (Vetex70, BRUKER, Germany) was collected in the region between 4000 and 450 cm^{-1}. The silica nanoparticles were mixed with potassium bromide (KBr). Thermo Gravimetric Analysis (TGA, TG1600, METTLER, Germany) test was performed from 30 to 900 °C at a heating rate of 10 °C min^{-1} under nitrogen atmosphere. Transmission electron microscopy (TEM) images were obtained using FEI Talos (F200X) equipped with a field emission gun and an accelerating voltage of 200 kV. The nanoparticles were dispersed in ethanol and a few drops of the solution was placed onto a lacey carbon covered copper grid. The solvent was evaporated at room temperature prior to observation. Differential scanning calorimetry (DSC, METTLER, Germany) was performed from 30 to 200 °C at a heating rate of 10 °C min^{-1} under nitrogen atmosphere. Tensile strength measurements were performed with a Universal Tensile Testing Machine (SANS ZMGI 250, China) with a loading rate of 10 mm min^{-1}. Liquid nitrogen fractured cross-section specimens were observed by scanning electron microscopy (SEM, VE-9800S, KEYENCE, Japan). Water absorption measurements were performed using a Microbalance (Adventurer SL AS 214, Ohaus, USA). The coating specimens were dried quickly using filter paper each time before weighing after the immersion 480 h in distilled water. Broadband dielectric spectroscopy (Concept 80, Novocontrol, Germany) was used to measure the dielectric parameters in a frequency range from 0.1 Hz to 1 MHz. Direct current (DC) resistivity was measured at room temperature by using a three-electrode electrometer (6517B, Keithley, USA) with an applied electric field of 1000 V mm^{-1}. Arc ablation resistance experiment was conducted at room temperature under a tailored high-voltage electrode system. The current applied on the specimen varies with the time as reported in our previous work [28]. The application of voltage stops when the arc extinguishes on the materials surface. The recorded duration time is the arc ablation resistance time. Alternating current (AC) electrical breakdown strength were measured in transformer oil at room temperature with a frequency of 50 Hz and a ramp rate of 1000 V s^{-1} using two opposite 25-mm diameter spherical copper electrodes.

3. Results and discussion

The FT-IR spectra of the OS, EGS, and epoxy resin are presented in Supporting Information Fig. S1. The EGS particles display the characteristic peaks that are not present in the OS particles but are seen in epoxy resin. Two overlapped peaks at 2967 cm^{-1} and 2926 cm^{-1} are assigned to the anti-symmetric stretching vibrations of methylene (—CH_2) and methyl (—CH_3) groups. The peak at 1509 cm^{-1} is attributed to the absorption of a carbon–carbon double bond (C═C) stretching vibration of the benzene ring. The peak at 912 cm^{-1} is assigned to the vibrations associated with the epoxide group. The peak at 834 cm^{-1} is attributed to the out-of-plane deformation of para-substituted benzene rings (=CH). Moreover, the stretching vibration peaks of the isocyanate group (-N═C═O) in the TDI molecules at 2271 cm^{-1} disappear on the spectrum. These results confirm that the TDI reacted completely to form the chemically-bonded interface between nanoparticles and epoxy molecules.

Supporting Information Fig. S2a shows the thermo-gravimetric curves of OS and EGS particles and Fig. S2b shows the maximum decomposition rate. The mass function of grafted TDI and epoxy molecules per unit mass of EGS particles is defined as grafting efficiency (E_g), which is given by

$$E_g = R_o - R_g \quad (1)$$

where E_g is the grafting efficiency, R_o is the mass loss rate of OS, and R_g is the mass loss rate of EGS. The mass losses of the two curves are almost coincident from the beginning to 250 °C, which is likely related to the dehydration of (Si—OH) and the removal of absorbed water on the nanoparticle surface. The less mass loss of EGS is attributed to the decrease in the number of hydroxyl groups on the nanoparticle surface as a result of the grafting modification. Notably, the mass loss of EGS particles dramatically increases between 300 and 550 °C, which is associated with the thermal decomposition of chemically-bonded organic layers on the surface. The mass loss rate of OS and EGS particles are about 6.8% and 20.4% at 900 °C, respectively, and the grafting efficiency of EGS particles is 16.2%. The morphology of nanoparticles evaluated by TEM is presented in Supporting Information Fig. S3, indi-

cating that the average particle size is around 30 nm. The glass transition temperature (T_g) of the samples are shown in Fig. 2 and the DSC curves are presented in Supporting Information Fig. S4. With the increase of filler content, T_gs for both OS and EGS composites increase initially and then decrease, which are likely due to the fact that the incorporated silica nanoparticles restrict the movement of epoxy chains as well as change the cross-linking density of the resultant composites. The EGS composites have the maximum T_g of 153.8 °C at 2.5 wt% filler loading, which is about 8.2 °C higher than neat epoxy. Interestingly, across the entire investigation range, T_g of the EGS composites is always higher than the OS composites with the same filler content. This is owing to the grafted epoxy groups on the surface of EGS particles that are involved in cross-linking reaction and subsequently result in greater hindrance of polymer chain motions.

The tensile strength and elongation at break for all the composites are shown in Fig. 3. The EGS-filled composites display the maximum tensile strength of 81.4 MPa and elongation at break of 3.38% at 2.5 wt% filler content, which is about 37% and 30% greater than neat epoxy resin, respectively. The mechanical strength of the EGS-filled composites is also greater than the OS-filled composites with the same filler content. In general, the mechanical properties of polymer composites are mainly affected by two conflicting factors induced by the incorporated nanoparticle: reinforcement and introduced defects. The former indicates that dispersed nanoparticles could act as stress concentrators to absorb some of the fracture energies and also inhibit the motion of polymer chains under mechanical loadings, thus presenting reinforcement behavior. On the other hand, the latter indicates that fillers are likely to form agglomerates and even introduce new interface defects, e.g. voids and micro-cracks, which decrease the tensile strength. Therefore, the mechanical strength of the composites is found to increase and then decrease with the increase of filler content.

The cross-sectional SEM images of the fracture microstructures of the composites are shown in Fig. 4. The fracture surface of neat epoxy is smooth with river-like lined cracks (Fig. 4a). The directions of cracks that cross the section are consistent, which is a typical characteristic of brittle fracture [29,30]. Compared with neat epoxy, the OS particles have minor effect on the direction of the cracks. A few agglomerates of the OS particles can be found in Fig. 4b. Large agglomerates emerge in Fig. 4d and Supporting Information Fig. S5a with high OS filler loadings. Conversely, as seen in Fig. 4c–e, there exist very few agglomerates in the epoxy/EGS nanocomposites, even at 2.5 wt% filler loading. It is found that numerous crazes spread through the propagation direction of cracks with fish-scaled patterns (Supporting Information Fig. S5b), which could block the extension of cracks and change the direction of the development of main cracks. The schematic illustrations of the epoxy/OS nanocomposite and the chemically-bonded cross-linked nets in the epoxy/EGS nanocomposite are shown in Fig. 4f and g, respectively. There are two main reasons for the differences in the fracture morphologies: First, the uniformly dispersed nanoparticles could act as stress concentrators to absorb a part of the fracture energy and initiate a higher degree of plastic deformation [6,31]. The chemically grafting modification effectively improves the compatibility of organic and inorganic phases, leading to better dispersion of EGS particles in epoxy matrix. The plastic deformation promotes local stress transfer between EGS particles and epoxy matrix, resulting in the emergence of surface crazes and a change in the crack direction. Second, the EGS particles with grafted epoxy chains not only offer the relatively stable physical bonding between EGS particles and epoxy matrix but also provide chemical-linkers between the epoxide-terminated EGS particles and the amino-terminated curing agent during the cross-linking reaction. The covalent bonds generate the enhanced interfacial adherence between EGS particles and epoxy matrix and dissipate more fracture energy under mechanical loading. Thus, the fracture morphology of epoxy/EGS nanocomposite is thought to be responsible for the improved mechanical strengths.

Additionally, the water absorption measurements confirm the tighter chemically-bonded structure in the epoxy−EGS interfaces in comparison with the epoxy−OS interfaces, which improves the compactness of materials and effectively hinders the process of water transport, as shown in Supporting Information Fig. S6. The saturated water absorption was calculated from three measurements that are given by

$$E_t = \frac{m_t - m_1}{m_1 - m_0} \times 100\% \quad (2)$$

where E_t defines the water absorption of the coating at a certain time, m_0 stands for the mass of free slides glass, m_1 is the mass of slides glass with coating before test and m_t represents the mass of slides glass with coating at a certain immersion time. The EGS particles exhibit strong hydrophobicity. On the other hand, the hydrophilic hydroxyls on the surface of the OS particles facilitate water absorption at the interface between OS particles and epoxy matrix. As a result, the incorporation of 1 wt% EGS particles into the epoxy matrix achieves the minimum saturated water absorption ratio of 2.08%, which is more than 34% and 29% reduction when compared with neat epoxy and the nanocomposite with 1 wt% OS, respectively. This improves the anti-aging property of epoxy materials by resisting water absorption.

The real part of permittivity (ε') and the loss tangent (tan δ) of the materials measured at room temperature are shown in Fig. 5. At relatively low filler contents, the ε' of the nanocomposite decrease with the increase of filler loading. The decrease in ε' is likely due to the restriction effect of nanofiller and the variation of free volume in the nanocomposites. The former indicates that the incorporated filler enhances the intermolecular interaction between nanoparticles and polymer matrix, which could restrict the movement of the dipole [32,33]. The latter proposed by Nelson [34] suggests that the free volume plays a dominant role in the value of ε' at low filler contents. The presence of the nanofillers generates free volumes in the epoxy nanocomposites, resulting in a reduction of ε'. Conversely, with further increase of filler content, both epoxy/OS and epoxy/EGS composites exhibit larger ε' than neat epoxy. This increase in ε' could be explained as follows [33]: First, the ε' value of silica, i.e. 4–4.5, is slightly larger than that of the host matrix, which gives rise to the growth of ε' in the nanocomposite. Second, the incorporated nanoparticles, especially the OS particles, might decrease the local cross-linking density, which subsequently increases the end- and side-chain percentages in the nanocomposites. Third, it is well-known that the polarization at low frequencies is attributable to the interfacial polarization. The existence of large agglomerations may exhibit more significant Maxwell–Wagner interfacial polarization than the nano-sized particles [35], which lead to a larger ε'. It is also worth noticing that the ε' of the epoxy/EGS nanocomposites, especially for 5 wt% filled at low frequencies, exhibits weaker frequency dependence than the epoxy/OS nanocomposites at the same filler loading, which is coincident with literature work [24]. This weak frequency dependence is suggestive of tighter chemically-bonded interface that can block the motion of epoxy chains and thus suppress the interfacial polarization. Moreover, the nanocomposites filled with EGS filler exhibit lower tan δ than OS filler, which could be due to the lower cross-linking density and more agglomerates in the OS-filled nanocomposites. Compared with the neat epoxy, the decreased tan δ in the EGS filled nanocomposites is likely owing to the wide-band-gap (~9 eV) silica fillers that function as charge-blocking insulators [36].

The electrical breakdown strength was determined from 15 samples and fitted with a 2-parameter Weibull distribution given by

$$P(E) = 1 - \exp\left(-(E/\alpha)^{\beta}\right) \quad (3)$$

where $P(E)$ is the probability of breakdown strength at a certain electric field strength and E is the measured electrical breakdown field. Scale parameter α is associated with the field strength at a 63.2% probability of breakdown. Shape parameter β represents the dispersion degree of the data. Larger values of β correspond to narrower data spreads. Fig. 6 shows the two-parameter Weibull plot of electrical breakdown strength of neat epoxy and the nanocomposites. The α and β parameters from the breakdown measurements were calculated and listed in Table 1.

The electrical breakdown strength is apparently affected by grafting modification. The EGS particles with chemically-bonded interface show a much pronounced reinforcement effect on the epoxy nanocomposite. In terms of Weibull breakdown strength, the nanocomposite with 2.5 wt% EGS displays the maximum improvement of 24%. In sharp contrast, the OS-filled nanocomposite exhibits a 1.3% reduction. Moreover, the enhancement of β is found in the EGS-filled nanocomposites, i.e., from 15.82 of neat epoxy to 24.12 of the nanocomposite with 2.5 wt% EGS, suggesting greatly improved dielectric reliability of the resultant nanocomposites. On the other hand, β value is decreased in the OS-filled nanocomposites, i.e. 11.36 at 2.5 wt% OS. In general, electrical breakdown strength could be affected by numerous factors. First, the electric resistivity of materials has an impact on the breakdown strength [37,38]. As shown in Fig. 7, the volume resistivity increases from the neat epoxy to the nanocomposites containing 0.3–1 wt% EGS filler, which is owing to the introduction of wide-band-gap fillers as well as the improvement of cross-linking densities. In contrast, due to the hydrophilic surface of OS nanoparticles, the electrical resistivity of the nanocomposite decreases with the increase of OS filler content. Second, the incorporation of nanoparticle could hinder carrier transport as well as block the extension of conductive tunnel. The chemically-bonded interface could improve the dispersion of nanoparticles and then shows more efficient hindrance to carrier transportation in the epoxy/EGS nanocomposite. The improvement of arc resistance time in the EGS-filled nanocomposites, as seen in Fig. 8, also demonstrate that the covalent bonds decrease the interfacial thermal resistance and effectively block the extension of conductive tunnel. The enhancement in arc resistance time is not obvious for the OS particles at relatively high filler contents. Third, the electromechanical failure is caused by mutual coulombic force from the opposite electrodes under an applied field, i.e., the higher the Young's modulus of the dielectric material, the better the material can withstand the coulombic force [37–39]. As seen in Supporting Information Fig. S7, the improvement of Young's modulus in the EGS-based nanocomposite contributes to the enhancement in breakdown strength. Fourth, the concentration and the mobility of charge carriers inside the nanocomposite influence the breakdown strength. The carrier concentration increases with the increase of shallow-trap density, whereas the carrier mobility decreases with the increase of deep-trap density. Meunier [40] proposed that shallow traps are likely to be generated by physical conformation defects whose energies are always lower than 0.3 eV, while deep traps (>1 eV) are always generated by chemical defects. Physical conformation defects are possibly introduced via the incorporation of OS particles due to the loose physically bonded interfaces between OS particles and epoxy matrix, generating shallow traps and increasing the carrier concentration. In contrast, the chemically-bonded interfaces between EGS particles and epoxy matrix are much tighter, making it easier for the generation of deep traps to reduce carrier mobility, improving the electrical breakdown strength.

It has been well-recognized that the organic–inorganic interface in the nanocomposite plays a prominent role in determining the dielectric properties of polymer composites [9,11,24–27,41–45]. Much improved fundamental understandings of the role of the interface are needed in order to design high-performance dielectric materials. For now, numerous interfacial theories and models have been proposed to understand the underlying mechanisms in dielectric polymer nanocomposites [32,46,47]. There are currently two widely accepted models: The Single-layer Structure Model by Lewis [46,47] and The Multi-Core Model by Tanaka [48]. Tanaka's model qualitatively explains the change of T_g, the decrease in dielectric constant and the inhibition of space charge. However, the mechanisms responsible for the variations of electrical breakdown strength of polymer nanocomposites are still lacking [49,50].

We propose the interaction zone models for the organic–inorganic interface in both epoxy/OS and epoxy/EGS composites to rationalize the experimental results of breakdown strength. The schematic diagrams of the growth of the discharge channel during the electrical breakdown process in epoxy resin and the nanocomposites are shown in Fig. 9. As demonstrated in Fig. 9a, the breakdown channel is almost in a single direction inside the neat epoxy. Fig. 9b shows that the breakdown channel is expended via the incorporation of OS particles. Moreover, as displayed in Fig. 9c, the expanded breakdown channels inside the epoxy/EGS composite are effectively lengthened in multiple directions as a result of a homogeneous distribution of the EGS particles. This is attributed to the favorable chemical bonding between EGS particles and the epoxy matrix, which restricts elongation of the breakdown channel. Fig. 9d shows that the proposed model for the interaction zone around the OS particles, which consists of a nanoparticle core, an untight region (UTR), and a polymer matrix. The interaction zone model for the EGS particles shown in Fig. 9e includes a nanoparticle, a tight chemically bonded region (CBR), an interfacial transition region (ITR), and a polymer matrix. The Fermi energy level of the interaction zone shall be different from that of both nanoparticles and polymer matrix. Thus, barriers could be formed at the interface of nanoparticle–CBR, CBR–ITR, and ITR–polymer matrix, respectively. Their barrier heights are assumed to reduce progressively from the inside out. Namely, the interaction between nanoparticle and polymer matrix is assumed to gradually become weaker, and accordingly, the trap energy gradually becomes shallower from the inside out. In the case of an ideal homogeneous distribution of nanoparticles, Li [32] assumed that the interaction zone and the nanoparticle occupy the same volume fraction. Hence, for the particle with a diameter of 30 nm, the thickness of the interaction zone is calculated to be 4 nm. At room temperature, the mean free path of most polymers is about a few nanometers [51], i.e., the thickness of the interaction zone should be less than the mean free path of the carrier. Under an applied electric field, it is difficult for the carrier to obtain sufficient energy to overcome the barrier of CBR–ITR after jumping into ITR. Thus, the carrier could not participate in the conduction process and the mobility of carrier is decreased, which is beneficial for breakdown strength of the polymer nanocomposite. With the increase of filler content, the space between the adjacent particles decreases and some interaction zones around the adjacent particles will be likely to overlap with each other. Thus, the thickness of the ITR will be greatly extended, and it could become larger than the mean free path of the carrier. Under such a condition, the carrier could obtain sufficient energy from the applied electric field to jump over the barrier of CBR–ITR so as to participate in conduction processes. The carrier could thus accumulate energy and participate in impact collision with defects in the polymer nanocomposites, reducing the electrical breakdown strength.

4. Conclusions

In this work, chemically-bonded surface layers for silica nanoparticles were prepared by grafting epoxy molecules. The resulting well-dispersed nanocomposites filled with the epoxy-grafted silica exhibit great enhancement in multiple physical properties, including the tensile strength, electrical breakdown strength, arc ablation resistance and water absorption resistance, compared with the neat epoxy and the

epoxy nanocomposites with unmodified silica. These results demonstrate that the chemically-bonded interfaces formed between the epoxy-grafted silica particles and the epoxy matrix effectively improve the compactness, mechanical strength and dielectric strength as well as water absorption resistance properties by circumventing particle aggregation, creating tight interphases and reducing interface defects. The interaction zone models for the polymer nanocomposites have been proposed, suggesting that the chemically-bonded interface not only hinders the transport of charge carriers but also generates deep traps to decrease the concentration and mobility of carriers, which helps to increase the electrical breakdown strength. This work further verifies the crucial role of organic–inorganic interface in determining the physical properties of polymer nanocomposites and sheds light on the development of high-performance dielectric polymer composites.

Acknowledgements

This work was supported by the National Natural Science Foundation of China (No. 51521065) and the Science and Technology Project of the State Grid Corporation of China (SGTYHT/15–JS–191). The authors would like to thank Lihua Feng and Zhenguo Zhang for their assistance in dielectric and thermal measurements. H. L. acknowledges the financial support from the China Scholarship Council (CSC).

Appendix A. Supplementary data

Supplementary data related to this article can be found at https://doi.org/10.1016/j.compscitech.2018.08.047.

References

[1] P. Mohan, A critical review: the modification, properties, and applications of epoxy resins, Polym. Plast. Technol. Eng. 52 (2) (2013) 107–125.
[2] Z. Lin, A. Mcnamara, Y. Liu, K.S. Moon, C.P. Wong, Exfoliated hexagonal boron nitride-based polymer nanocomposite with enhanced thermal conductivity for electronic encapsulation, Compos. Sci. Technol. 90 (2014) 123–128.
[3] H. Li, C. Wang, Z. Guo, H. Wang, S. Zhang, Z. Peng, et al., Influences of semi-conductive coatings on the electric field distribution of GIS spacer interface, Properties and Applications of Dielectric Materials, In: IEEE International Conference on the (ICPADM), 2015, pp. 887–890.
[4] K. Lee, K. Lee, Y. Choi, D. Park, K. Lim, Improved thermal, structural and electrical properties of epoxy for use at high voltages, IEEE Trans. Dielectr. Electr. Insul. 12 (3) (2005) 566–572.
[5] C. Wang, H. Li, H. Zhang, H. Wang, L. Liu, Z. Xu, et al., Influence of addition of hydroxyl-terminated liquid nitrile rubber on dielectric properties and relaxation behavior of epoxy resin, IEEE Trans. Dielectr. Electr. Insul. 23 (4) (2016) 2258–2269.
[6] L. Dong, W. Zhou, X. Sui, Z. Wang, H. Cai, P. Wu, et al., A carboxyl-terminated polybutadiene liquid rubber modified epoxy resin with enhanced toughness and excellent electrical properties, J. Electron. Mater. 45 (7) (2016) 3776–3785.
[7] L. Qi, B.I. Lee, S. Chen, W.D. Samuels, G.J. Exarhos, High-dielectric-constant silver–epoxy composites as embedded dielectrics, Adv. Mater. 17 (14) (2005) 1777–1781.
[8] P.C. Ma, J.-K. Kim, B.Z. Tang, Effects of silane functionalization on the properties of carbon nanotube/epoxy nanocomposites, Compos. Sci. Technol. 67 (14) (2007) 2965–2972.
[9] X. Huang, Y. Zheng, P. Jiang, Y. Yin, Influence of nanoparticle surface treatment on the electrical properties of cycloaliphatic epoxy nanocomposites, IEEE Trans. Dielectr. Electr. Insul. 17 (2) (2010) 635–643.
[10] S. Zhao, L.S. Schadler, R. Duncan, H. Hillborg, T. Auletta, Mechanisms leading to improved mechanical performance in nanoscale alumina filled epoxy, Compos. Sci. Technol. 68 (14) (2008) 2965–2975.
[11] W. Peng, X. Huang, J. Yu, P. Jiang, W. Liu, Electrical and thermophysical properties of epoxy/aluminum nitride nanocomposites: effects of nanoparticle surface modification, Compos. Part A: Appl. Sci. Manuf. 41 (9) (2010) 1201–1209.
[12] Y. Niu, Y. Bai, K. Yu, L. He, F. Xiang, H. Wang, Fabrication, structure, and property of epoxy-based composites with metal–insulator core–shell structure fillers, J. Mater. Res. 28 (18) (2013) 2644–2649.
[13] J. Chen, X. Huang, Y. Zhu, P. Jiang, Cellulose nanofiber supported 3D interconnected BN nanosheets for epoxy nanocomposites with ultrahigh thermal management capability, Adv. Funct. Mater. 27 (5) (2017), 1604754.
[14] Z.-M. Dang, Y.-F. Yu, H.-P. Xu, J. Bai, Study on microstructure and dielectric property of the $BaTiO_3$/epoxy resin composites, Compos. Sci. Technol. 68 (1) (2008) 171–177.
[15] S. Luo, Y. Shen, S. Yu, Y. Wan, W.-H. Liao, R. Sun, et al., Construction of a 3D-$BaTiO_3$ network leading to significantly enhanced dielectric permittivity and energy storage density of polymer composites, Energy Environ. Sci. 10 (1) (2017) 137–144.
[16] F. Meng, L. Liu, W. Tian, H. Wu, Y. Li, T. Zhang, et al., The influence of the chemically bonded interface between fillers and binder on the failure behaviour of an epoxy coating under marine alternating hydrostatic pressure, Corrosion Sci. 101 (2015) 139–154.
[17] X. Wang, L. Wang, Q. Su, J. Zheng, Use of unmodified SiO_2 as nanofiller to improve mechanical properties of polymer-based nanocomposites, Compos. Sci. Technol. 89 (2013) 52–60.
[18] G.D. Smith, D. Bedrov, Dispersing nanoparticles in a polymer matrix: are long, dense polymer tethers really necessary?, Langmuir 25 (19) (2009) 11239–11243.
[19] M. Rong, M. Zhang, W. Ruan, Surface modification of nanoscale fillers for improving properties of polymer nanocomposites: a review, Mater. Sci. Technol. 22 (7) (2006) 787–796.
[20] S. Kango, S. Kalia, A. Celli, J. Njuguna, Y. Habibi, R. Kumar, Surface modification of inorganic nanoparticles for development of organic–inorganic nanocomposites—a review, Prog. Polym. Sci. 38 (8) (2013) 1232–1261.
[21] L. Xing, Q. Li, G. Zhang, X. Zhang, F. Liu, L. Liu, et al., Self-healable polymer nanocomposites capable of simultaneously recovering multiple functionalities, Adv. Funct. Mater. 26 (20) (2016) 3524–3531.
[22] Y. Wang, J. Cui, L. Wang, Q. Yuan, Y. Niu, J. Chen, et al., Compositional tailoring effect on electric field distribution for significantly enhanced breakdown strength and restrained conductive loss in sandwich-structured ceramic/polymer nanocomposites, J. Mater. Chem. A 5 (9) (2017) 4710–4718.
[23] X. Liu, F. Xu, K. Zhang, B. Wei, Z. Gao, Y. Qiu, Characterization of enhanced interfacial bonding between epoxy and plasma functionalized carbon nanotube films, Compos. Sci. Technol. 145 (2017) 114–121.
[24] A. Xie, Y. Wang, P. Jiang, S. Li, X. Huang, Nondestructive functionalization of carbon nanotubes by combining mussel-inspired chemistry and RAFT polymerization: towards high dielectric nanocomposites with improved thermal management capability, Compos. Sci. Technol. 154 (2018) 154–164.
[25] Y. Niu, Y. Bai, K. Yu, Y. Wang, F. Xiang, H. Wang, Effect of the modifier structure on the performance of barium titanate/poly (vinylidene fluoride) nanocomposites for energy storage applications, ACS Appl. Mater. Interfaces 7 (43) (2015) 24168–24176.
[26] Y. Niu, F. Xiang, Y. Wang, J. Chen, H. Wang, Effect of the coverage level of carboxylic acids as a modifier for barium titanate nanoparticles on the performance of poly (vinylidene fluoride)-based nanocomposites for energy storage applications, Phys. Chem. Chem. Phys. 20 (9) (2018) 6598–6605.
[27] H. Li, C. Wang, Z. Guo, H. Wang, Y. Zhang, R. Hong, et al., Effects of silane coupling agents on the electrical properties of silica/epoxy nanocomposites, In: IEEE Int. Conf. Dielectr. (ICD), 2016, pp. 1036–1039.
[28] Z. Guo, H. Wang, H. Li, C. Wang, X. Lv, Z. Peng, Experiment study on arc ablation resistance performance of epoxy with alumina fillers, In: IEEE Int. Conf. Prop. Appl. Dielectr. Mater., (ICPADM), 2015, pp. 620–623.
[29] D. Pinto, L. Bernardo, A. Amaro, S. Lopes, Mechanical properties of epoxy nanocomposites using titanium dioxide as reinforcement–a review, Construct. Build. Mater. 95 (2015) 506–524.
[30] L. Dong, W. Zhou, X. Sui, Z. Wang, H. Cai, P. Wu, et al., Mechanical and electrical properties of aluminum/epoxy nanocomposites, J. Electron. Mater. 45 (11) (2016) 5885–5894.
[31] R. Thomas, D. Yumei, H. Yuelong, Y. Le, P. Moldenaers, Y. Weimin, et al., Miscibility, morphology, thermal, and mechanical properties of a DGEBA based epoxy resin toughened with a liquid rubber, Polymer 49 (1) (2008) 278–294.
[32] S. Li, G. Yin, S. Bai, J. Li, A new potential barrier model in epoxy resin nanodielectrics, IEEE Trans. Dielectr. Electr. Insul. 18 (5) (2011).
[33] S. Singha, M.J. Thomas, Dielectric properties of epoxy nanocomposites, IEEE Trans. Dielectr. Electr. Insul. 15 (1) (2008).
[34] J.K. Nelson, Y. Hu, The impact of nanocomposite formulations on electrical voltage endurance, Solid Dielectrics, In: IEEE International Conference on (ICSD), 2004, pp. 832–835.
[35] J.K. Nelson, J.C. Fothergill, Internal charge behaviour of nanocomposites, Nanotechnology 15 (5) (2004) 586.
[36] P. Peacock, J. Robertson, Band offsets and Schottky barrier heights of high dielectric constant oxides, J. Appl. Phys. 92 (8) (2002) 4712–4721.
[37] Q. Li, G. Zhang, F. Liu, K. Han, M.R. Gadinski, C. Xiong, et al., Solution-processed ferroelectric terpolymer nanocomposites with high breakdown strength and energy density utilizing boron nitride nanosheets, Energy Environ. Sci. 8 (3) (2015) 922–931.
[38] Q. Li, F. Liu, T. Yang, M.R. Gadinski, G. Zhang, L.-Q. Chen, et al., Sandwich-structured polymer nanocomposites with high energy density and great charge–discharge efficiency at elevated temperatures, Proc. Natl. Acad. Sci. Unit. States Am. 113 (36) (2016) 9995–10000.
[39] M. Ieda, Dielectric breakdown process of polymers, IEEE Trans. Dielectr. Electr. Insul., EI- 15 (3) (1980) 206–224.
[40] M. Meunier, N. Quirke, Molecular modeling of electron trapping in polymer insulators, J. Chem. Phys. 113 (1) (2000) 369–376.
[41] M. Roy, J. Nelson, R. MacCrone, L.S. Schadler, C. Reed, R. Keefe, Polymer nanocomposite dielectrics-the role of the interface, IEEE Trans. Dielectr. Electr. Insul. 12 (4) (2005) 629–643.

[42] J. Li, J. Claude, L.E. Norena-Franco, S.I. Seok, Q. Wang, Electrical energy storage in ferroelectric polymer nanocomposites containing surface-functionalized $BaTiO_3$ nanoparticles, Chem. Mater. 20 (20) (2008) 6304–6306.
[43] K. Han, Q. Li, Z. Chen, M.R. Gadinski, L. Dong, C. Xiong, et al., Suppression of energy dissipation and enhancement of breakdown strength in ferroelectric polymer–graphene percolative composites, J. Mater. Chem. C 1 (42) (2013) 7034–7042.
[44] X. Huang, L. Xie, K. Yang, C. Wu, P. Jiang, S. Li, et al., Role of interface in highly filled epoxy/$BaTiO_3$ nanocomposites. Part II-effect of nanoparticle surface chemistry on processing, thermal expansion, energy storage and breakdown strength of the nanocomposites, IEEE Trans. Dielectr. Electr. Insul. 21 (2) (2014) 480–487.
[45] G. Zhang, D. Brannum, D. Dong, L. Tang, E. Allahyarov, S. Tang, et al., Interfacial polarization-induced loss mechanisms in polypropylene/$BaTiO_3$ nanocomposite dielectrics, Chem. Mater. 28 (13) (2016) 4646–4660.
[46] T. Lewis, Interfaces are the dominant feature of dielectrics at the nanometric level, IEEE Trans. Dielectr. Electr. Insul. 11 (5) (2004) 739–753.
[47] T. Lewis, Interfaces: nanometric dielectrics, J. Phys. D Appl. Phys. 38 (2) (2005) 202.
[48] T. Tanaka, M. Kozako, N. Fuse, Y. Ohki, Proposal of a multi-core model for polymer nanocomposite dielectrics, IEEE Trans. Dielectr. Electr. Insul. 12 (4) (2005) 669–681.
[49] C.A. Grabowski, S.P. Fillery, N.M. Westing, C. Chi, J.S. Meth, M.F. Durstock, et al., Dielectric breakdown in silica–amorphous polymer nanocomposite films: the role of the polymer matrix, ACS Appl. Mater. Interfaces 5 (12) (2013) 5486–5492.
[50] M. Bell, T. Krentz, J.K. Nelson, L.S. Schadler, K. Wu, C. Breneman, et al., Investigation of dielectric breakdown in silica-epoxy nanocomposites using designed interfaces, J. Colloid Interface Sci. 495 (2017) 130–139.
[51] G. Dlubek, J. Stejny, T. Lüpke, D. Bamford, K. Petters, C. Hübner, et al., Free-volume variation in polyethylenes of different crystallinities: positron lifetime, density, and X-ray studies, J. Polym. Sci. B Polym. Phys. 40 (1) (2002) 65–81.